Applied Catalysis B: Environmental 259 (2019) 118051

Contents lists available at ScienceDirect

Applied Catalysis B: Environmental

journal homepage: www.elsevier.com/locate/apcatb

A unique amorphous cobalt-phosphide-boride bifunctional electrocatalyst for enhanced alkaline water-splitting

A. Chunduri[a], S. Gupta[b,*], O. Bapat[a], A. Bhide[a], R. Fernandes[a], M.K. Patel[b], V. Bambole[a], A. Miotello[c], N. Patel[a,*]

[a] Department of Physics, University of Mumbai, Vidyanagari, Santacruz (E), Mumbai, 400098, India
[b] School of Engineering, University of Liverpool, Brownlow Hill, L69 3GH, Liverpool, United Kingdom
[c] Dipartimento di Fisica, Università degli Studi di Trento, I-38123, Povo, Trento, Italy

ARTICLE INFO

Keywords:
Cobalt-phosphide-boride
Non-noble electrocatalyst
Bifunctional water-splitting
H-adsorption energy
Alkaline water electrolysis

ABSTRACT

A unique cobalt-phosphide-boride (Co-P-B) catalyst was synthesized via simple chemical-reduction route. The obtained catalyst was amorphous in nature, resembling the spherical morphology of Co-B nanoparticles. X-ray photoelectron spectroscopy revealed that B loses electrons to Co while P gains electrons from Co. This unique electron transfer mechanism in Co-P-B is a combination of the characteristics showcased by Co-B and Co-P catalysts individually. The optimized catalyst (Co-P-B-5) showed overpotentials of 145 mV and 290 mV to achieve the benchmark current density of 10 mA/cm^2 for HER and OER, respectively, in 1 M NaOH. From theoretical calculations, it was observed that addition of P modulates the electron density at Co sites, thereby optimizing the H-adsorption capability, leading to higher HER rate. During anodic polarization, Co-P-B-5 shows formation of large number of CoOOH species on its surface, facilitating OER. Finally, stability, recyclability and wide-pH suitability of Co-P-B-5 was established to demonstrate its industrial viability.

1. Introduction

Developing hydrogen-based technologies [1,2] will play a key role in reducing the ecological and demographic impacts induced by fossil fuels. Amongst various available methods, electrochemical water-splitting is one of the cleanest ways to produce industrial grade hydrogen (H_2) by using surplus energy of renewable sources [1]. The complete water-splitting mechanism involves hydrogen evolution reaction (HER) and oxygen evolution reaction (OER) taking place on cathode and anode sides of the electrolyser, respectively [3–5]. By using appropriate catalyst materials for the fabrication of these electrodes, water-splitting reaction can be carried out close to its thermoneutral voltage. The present technology of water electrolyzers rely completely on precious and rare-earth based electrodes (Pt, RuO_2, Pd, IrO_2, etc.), which limits its wide-scale implementation [6]. In order to substitute these precious catalysts, low-cost and earth-abundant electrode materials with similar efficiency have been discovered [3,4].

Over the last decade, non-noble transition-metal catalysts based on phosphides [7,8], borides [9,10], sulphides [11,12], selenides [13,14] and carbides [15,16] have been reported to be highly efficient in catalysing the water-splitting reaction, competing well with Pt and other precious catalysts. In particular, transition-metal phosphides (Co-P [17], Ni-P [18], Mo-P [19], etc.) and borides (Co-B [9], Ni-B [10], Fe-B [20], etc.) have shown exceptional performances towards HER as well as OER in multiple pH solutions. The higher HER rate in metal phosphides, like Co-P, is ascribed to the “ensemble effect”, where P attains a negative charge density, owing to the transfer of electrons from Co and acts as the active centre [7,21]. On the contrary, the superior performance of borides, like Co-B, is ascribed to an exactly opposite phenomena, owing to the reverse electron transfer mechanism [9,22], where B loses electrons to Co, thereby making it rich in electrons and thus improving the HER rate. The charge transfer from B to Co (the latter element has lower electronegativity than B) is related to the disordered structure of the Co-B compound and has been proved both experimentally by X-Photoelectron Spectroscopy and theoretically on the basis of the density functional theory (DFT) [9]. To combine the advantages of these two materials, both P and B can be coupled to Co giving rise to cobalt phosphide boride (Co-P-B) catalysts.

Recently Co-P-B/rGO [23] composites were reported for their HER and OER performance in neutral medium. Amorphous Co-P-B was also studied for its HER performance in acidic [24] and alkaline [25] medium by two different groups. However, no report has ever been made to explore the bifunctional characteristic of Co-P-B catalyst in alkaline medium. As a major share of industrial water electrolyzers are

* Corresponding authors.
E-mail addresses: Suraj.Gupta@liverpool.ac.uk (S. Gupta), nainesh11@gmail.com (N. Patel).

https://doi.org/10.1016/j.apcatb.2019.118051
Received 28 February 2019; Received in revised form 30 July 2019; Accepted 3 August 2019
Available online 05 August 2019
0926-3373/

used under extremely alkaline conditions, it is important to test the new electrode materials under these conditions. Also, from the present literature, the role of P and B in individual Co-P and Co-B are understood, but the combined synergistic effects created by inclusion of P and B in Co-P-B are not clear. This is crucial in designing new catalysts based on the Co-P-B system. In this regard, correlating the experimental results with that obtained through computational tool makes a huge difference in understanding the part played by each of the constituents. As mentioned previously, our group used DFT to validate the phenomena of reverse electron transfer in amorphous cobalt boride, thereby predicting Co to be the active centre for HER [9]. Similarly, by using experimental and computational results, the role of Ni in further enhancing the activity of Co sites in Co-Ni-B was determined [26]. DFT studies were performed by many groups [20,27,28] to identify the H-adsorption energies on various sites, giving information about the favourable surface sites for an experimentally active catalyst. Such combined methods can be used to understand the reasons for higher reaction rates in various materials, which is often neglected by researchers working in the area of electrocatalytic water-splitting. Finally, the common route of synthesis for Co-P-B catalyst employs high temperature phosphidation and a more simple and safe method is required.

In order to address the above issues, the current work uses a combined experimental and computational approach to develop Co-P-B electrocatalyst using a non-toxic method. These catalysts have vastly improved HER and OER performances compared to Co-B and Co-P. Various characterization techniques and DFT studies were used to understand the reasons behind higher reaction rates for HER as well as OER in Co-P-B. In the end, stability and wide-pH suitability of the catalyst was also demonstrated, making Co-P-B an attractive proposition for industrial electrolyzers.

2. Experimental details

2.1. Synthesis of catalyst powders

Chemical reduction method was used to synthesize the desired catalysts. An aqueous solution of cobalt chloride hexahydrate ($CoCl_2.6H_2O$, 0.05 M) and sodium hypophosphite (NaH_2PO_2) was prepared. Under vigorous stirring, sodium borohydride ($NaBH_4$) was added to the above solution. To ensure complete reduction of cobalt chloride, the molar ratio of (B + P)/Co was kept three for all experiments. As the reaction is spontaneous, effervescence is noticed due to liberation of H_2 gas and the solution turns black immediately. This mixture is continuously stirred for 15 min until the effervescence ceases. The resulting mixture is centrifuged to separate the black powder and is washed thoroughly with double distilled water (DDW) and then finally with alcohol to remove the remnant impurities. To obtain different molar ratio of B/P in Co-P-B catalyst, the molar concentrations of $NaBH_4$ and NaH_2PO_2 were varied. Co-B powder was also synthesized using a similar method, without using NaH_2PO_2.

Co-P powder was synthesized using $CoCl_2.6H_2O$ (0.1 M) as the precursor while NaH_2PO_2 (1 M) was used as the reducing agent. The reaction temperature is maintained at 90 °C and pH is adjusted to 11 with the help of 30 wt.% NaOH aqueous solution. After 30 min of vigorous stirring, the resulting black powder was first washed with 8% aqueous ammonia and then repeatedly washed with DDW and finally with alcohol to ensure complete removal of the impurities.

2.2. Characterization of catalyst powders

Surface morphology of the catalyst powders was investigated using scanning electron microscopy (SEM) (FEI INSPECT F50) and Transmission electron microscope (TEM) (FEI Tecnai G2, F30, 300 kV). HR–TEM images and selective area electron diffraction (SAED) patterns were also obtained to determine the particle size distribution and crystallinity of the prepared catalyst powders. Structural characterization of the catalyst powders was done by X-Ray Diffraction (XRD) (Rigaku Ultima IV, Cu K_α radiation with $\lambda = 1.5414$ Å) in θ-2θ configuration. To determine the surface area of the catalyst powders, a multi-point BET with N_2 adsorption method was used. The adsorption-desorption isotherms were obtained after 2 h of degassing the samples at 423 K. To study the composition and electronic states of the catalyst surface, X-ray photo-electron spectroscopy (XPS) (PHI 5000 Versaprobe-II) was used. XPS data was recorded at room temperature using spectrophotometer calibrated with Au $4f_{7/2}$ line positioned at 83.8 eV. Al K_α radiation at 1486.6 eV was used for ejecting the photoelectrons from the sample surface. The C 1s line positioned at 284.8 eV was recorded during each scan as internal calibration to ensure the absence of any charging effect. Inductive coupled plasma – Atomic Emission Spectroscopy (ICP-AES) (SPECTRO Analytical Instruments GmbH) was used to quantify the elemental composition of the developed catalysts. To carry out post-HER and post-OER characterizations, the sample was scraped off from the surface of glassy carbon electrode after long-term potentiostatic tests for HER and OER.

2.3. Preparation of electrodes

3 mm glassy carbon (GC) electrode (CH instruments) was used for the deposition of catalyst powders. For deposition, well dispersed homogenous ink was prepared by sonication of each catalyst powder (2 mg) in 2 ml ethanol. 20 µl of Nafion (5%) was sonicated in 0.5 ml of ethanol to prepare a homogenous binder solution. On polished GC, initially 10 µl of Nafion binder solution is drop-casted evenly and dried under IR lamp. After this layer, 20 µl of catalyst ink is drop-casted uniformly and dried under IR lamp. A catalyst loading of 0.3 mg/cm^2 was maintained for all the depositions.

2.4. Electrochemical measurements

For electrochemical activity measurements, a potentiostat system from CH instruments (660D) was used with a 3-electrode cell configuration. Catalyst loaded GC was used as the working electrode, a saturated calomel electrode as reference and a Pt electrode (CH Instruments) was used as counter. 1 M NaOH (pH 14) was used as the electrolyte for all measurements. For measurements in acidic and neutral media, 0.1 M $HClO_4$ and 0.5 M potassium phosphate (KPi) solutions were used, respectively. Prior to polarization measurements for HER, a potentiostatic sweep was conducted until the resultant current is stabilised. This ensures removal of any oxidation layer formed on the catalyst surface. All the linear polarization measurements for both HER and OER were performed at a scan rate of 10 mV/s. For all the catalyst powders, uncompensated resistance (R_s) was determined with the help of impedance spectroscopy (Nyquist plot) and the same value was used for overpotential (η) calculations. All the potentials were converted to reversible hydrogen electrode (RHE) by adding the value of 1.068 (for pH14) obtained from Nernst equation $E = E^o + (0.059*pH)$ where $E^o = 0.241$ V for saturated calomel electrode [29]. From the plot of "log (i) vs η", Tafel slope and exchange current density values were obtained. Turnover frequency (TOF) values were calculated using the procedure mentioned in a previous work [26]. Cyclic voltammetry (CV) scans were performed for Co-P-B (B/P = 5), Co-B and Co-P in 1 M NaOH to determine the electrochemically active surface area. For this purpose, CV scans at different scan rates (20, 40, 60, 80, 100 mV/sec) were performed within the potential range of -0.35 to -0.15 V (vs RHE). From these plots, the difference in anodic and cathodic current densities (Δj) at -0.25 V (vs RHE) was plotted against the corresponding scan rates. The slope of the line obtained by linear fit is twice the value of the double layer capacitance (C_{DL}) at the interface of electrolyte and catalyst [30].

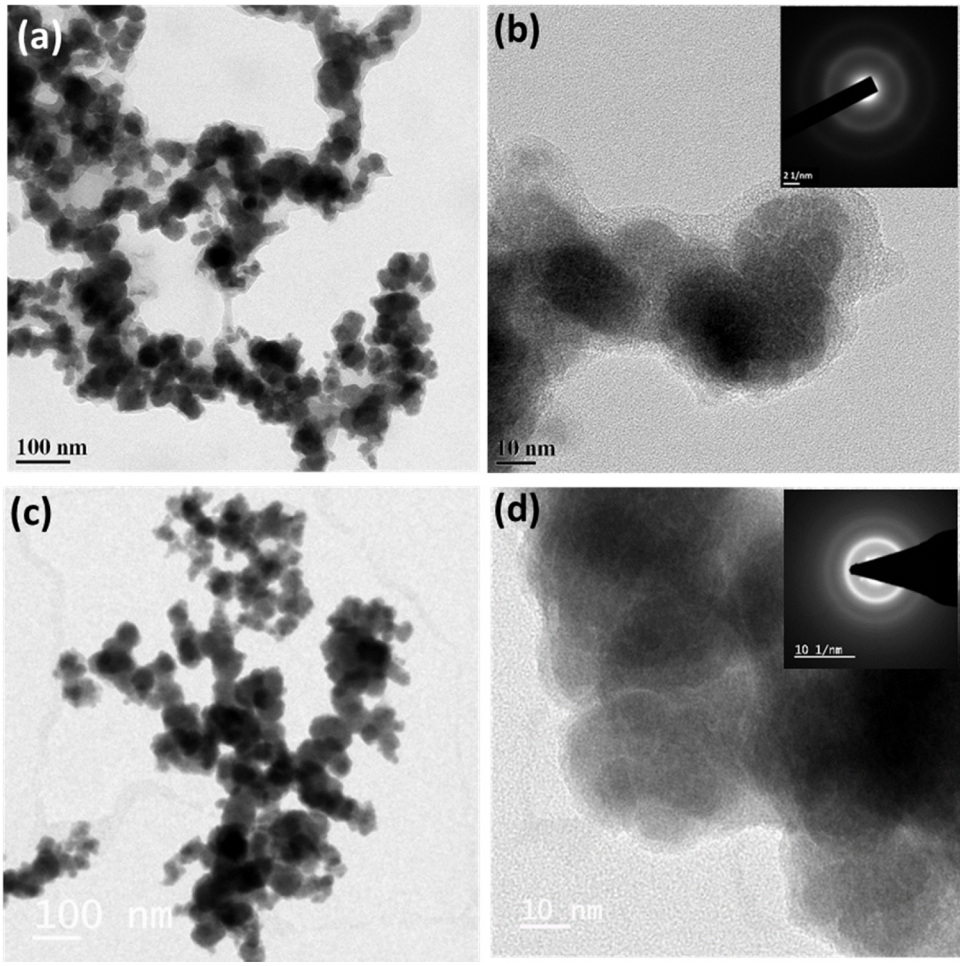

Fig. 1. TEM images of **(a)** Co-B, **(c)** Co-P-B-5 and HRTEM images of **(b)** Co-B, **(d)** Co-P-B-5. Inset in HRTEM images shows SAED patterns indicating amorphous nature of the catalysts.

3. Results and discussion

The molar ratio of B/P in Co-P-B was optimized in terms of catalytic activity, and it was found that the catalyst with B/P = 5 (termed as Co-P-B-5) showed the best electrocatalytic performance (discussed later). Hence, Co-P-B-5 was considered for all physical characterizations. **Fig. S1** shows SEM images of Co-B, Co-P and Co-P-B-5 catalysts. It can be seen that Co-P has nano-flake like morphology whereas Co-B and Co-P-B-5 exist as agglomerated spherical particles. During synthesis of Co-B and Co-P-B-5, $NaBH_4$ was used, which is comparatively a much stronger reducing agent than NaH_2PO_2. Hence, the reduction process is instantaneous with $NaBH_4$, resulting in agglomeration, owing to the high surface energy of formed nanoparticles. TEM micrographs obtained for Co-B and Co-P-B-5 are shown in Fig. 1. From Fig. 1**a** and **c**, it is clearly evident that both the catalysts show formation of spherical particles with average size in the range of 30–50 nm. The degree of agglomeration appears slightly more in the case of Co-P-B-5 (Fig. 1**d**). From their corresponding HR-TEM images (Fig. 1**b** and **d**), one can see that both the catalysts are completely amorphous and do not show presence of any crystalline phases/lattice planes. This amorphous nature is also confirmed by the occurrence of diffused rings, as observed in their respective SAED patterns (inset of Fig. 1**b** and **d**).

To validate the observation of amorphous nature from TEM, XRD was used and the corresponding diffractograms are shown in **Fig. S2**. As seen from the figure, Co-P-B-5 and Co-B catalysts show absence of any crystalline peaks and only an amorphous hump close to $2\theta = 45^\circ$ is observed, consistent with previous reports on amorphous Co-based borides [9,26,29]. Co-P shows characteristic diffraction peaks at 31.7°, 37.8°, 48.1° and 57.7°, which are assigned to (011), (111), (211) and (020) planes of orthorhombic Co-P (JCPDS: 00-029-0497) [10], suggesting formation of pure Co-P phase.

The chemical states of the developed catalysts were investigated by using XPS spectra (Fig. 2). The survey spectra of Co-P-B-5 shows presence of Co, P, B and O with no other impurities (**Fig. S3**). The existence of O in the survey spectrum is due to the exposure of the samples to ambient atmosphere during measurement. The XPS spectra of Co $2p_{3/2}$ states for Co-B (Fig. 2a) and Co-P-B-5 (Fig. 2c) can be deconvoluted into peaks corresponding to metallic and oxidized cobalt. The binding energy (BE) peak at 778.1 eV corresponds to metallic Co while the one at 781.0 eV (for Co-B) and 781.1 eV (for Co-P-B-5) corresponds to oxidized divalent cobalt [31]. A shake-up satellite peak in the higher BE range corresponding to divalent Co also appears in both cases. For Co-P (Fig. 2b), no signature of metallic Co is observed, instead it shows peaks at 780.6 eV and 782.4 eV, corresponding to divalent and trivalent Co [32]. In case of B 1 s states, both Co-B (Fig. 2d) and Co-P-B-5 (Fig. 2e) show BE peaks at 188.0 eV corresponding to elemental boron. However, BE of these peaks are positively shifted by 0.9 eV, when compared to that of pure B (187.1 eV), indicating partial loss of electrons from boron. This electronic transfer is commonly observed for amorphous metal borides (Co-B, Ni-B) [9,22,25]. In both the samples, a higher energy peak corresponding to oxidized boron is also observed.

The 2p level of phosphorous in Co-P is deconvoluted into three peaks with positions at 127.7 eV, 132.9 eV and 135.1 eV (Fig. 2f). Among these, the peak positions at 132.9 eV and 135.1 eV are assigned

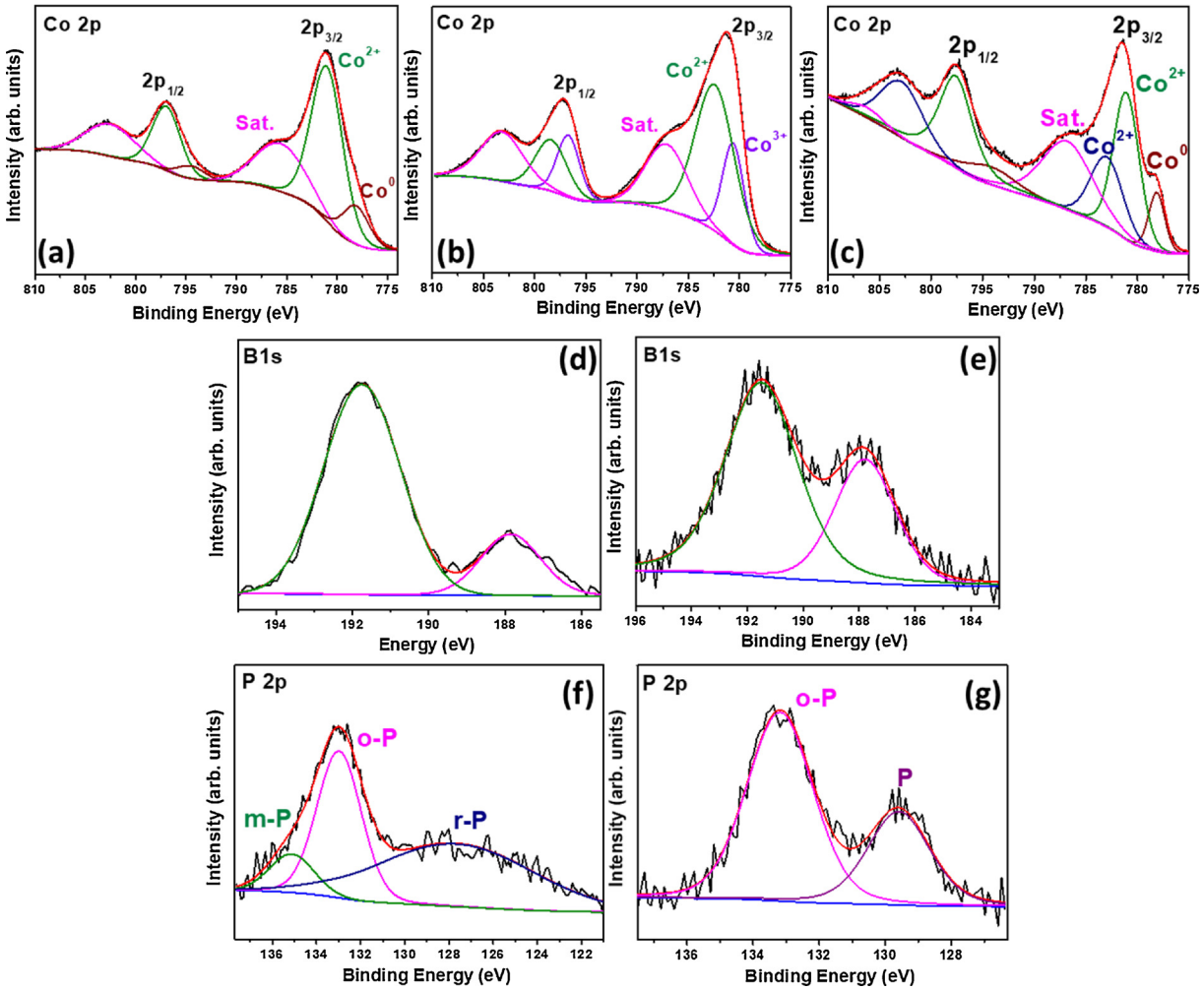

Fig. 2. XPS spectra for Co 2p states in **(a)** Co-B, **(b)** Co-P, **(c)** Co-P-B-5; B 1 s states in **(d)** Co-B, **(e)** Co-P-B-5 and P 2p states in **(f)** Co-P, **(g)** Co-P-B-5.

to orthophosphate and metaphosphate [10] respectively, while the peak at 127.7 eV is assigned to reduced phosphorous [33]. On the other hand, the 2p level of phosphorous in Co-P-B is deconvoluted into two kinds of species with BE of 129.6 eV and 133.2 eV (Fig. 2g). In this doublet, the peak at 129.6 eV is attributed to metallic phosphorous (P^0) and the other peak at 133.2 eV is ascribed to oxidized phosphorus [31,33] (orthophosphate). When the metallic P^0 peak of Co-P-B-5 is compared to that of pure P (130.2 eV), a negative shift of 0.6 eV is observed, indicating partial electron-transfer towards P. Such a phenomenon is usually observed in Co-P catalyst, owing to the so-called 'ensemble effect' [7,21]. It is quite interesting to note here that the electron-transfer mechanism in Co-P-B-5 is analogous to that observed in Co-B (electron loss from B) as well as in Co-P (electron gain by P). This electronic transfer renders unique electronic characteristics to Co-P-B-5 that may facilitate water-splitting reactions. Surface elemental composition was also determined from XPS, as shown in **Table S1**. ICP-AES was used to quantify the bulk chemical composition of as prepared Co-B, Co-P-B-5 and Co-P catalysts, as reported in **Table S1**. On comparing the surface and bulk elemental concentrations, it is observed that the catalysts containing P (Co-P-B-5 and Co-P) show an enrichment of Co atoms on their surface.

The electrochemical performance of the developed catalysts was evaluated by testing them in 1 M NaOH (pH 14) for HER as well as OER. The value of uncompensated resistance (R_s) was determined by fitting the Nyquist curves obtained from impedance spectroscopy and was subtracted from the raw data. Hereon, all the potentials are referenced to RHE, unless stated otherwise. **Fig. S4** shows LSV curves for Co-P-B catalyst with different ratios of B/P, namely B/P = 1, 3, 5 and 7. It was found that the ratio of B/P = 5 shows the best electrochemical activity for HER (**Fig. S4a**) as well as OER (**Fig. S4b**), in pH 14. Fig. 3**a** compares the HER activity of Co-P-B-5 with that of Co-B, Co-P and Pt catalyst. To achieve the benchmark current density of 10 mA/cm^2, an overpotential of 145 mV is required by Co-P-B-5, which is about 100 mV lower than that of Co-B catalyst (249 mV). The Tafel slope for Co-P-B-5 (38 mV/dec) is similar to Pt (39 mV/dec) and is lower than that of Co-B (42 mV/dec) (Fig. 3b). This suggests that though the reaction mechanism over both the catalysts is the same (Volmer-Heyrovsky) [34,35], the reaction proceeds over Co-P-B-5 in a more efficient manner. Additionally, the calculated exchange current density for Co-P-B-5 is much higher (5.93 mA/cm^2) than that of Co-B (0.097 mA/cm^2). Co-P shows very meagre HER activity which might be due to the unconventional synthesis method adopted here.

Most of the Co-based borides and phosphides have been reported as equally efficient in catalysing the water oxidation reaction. Hence, the electrochemical performance of Co-P-B-5 was tested under anodic polarization in pH 14. Fig. 3**c** shows the linear sweep curves of Co-P-B-5, Co-B, Co-P and standard RuO_2 catalyst in pH 14, recorded at a scan rate of 10 mV/s, while Fig. 3**d** shows the corresponding Tafel plots. Co-P-B-5 exhibits the most superior OER activity, which supersedes that of Co-B, Co-P as well as RuO_2. To achieve 10 mA/cm^2, an overpotential of 290 mV, 340 mV, 340 mV and 380 mV is required by Co-P-B-5, Co-B, Co-P and RuO_2, respectively, demonstrating the highly improved performance of Co-P-B-5. Even at higher current densities of 100 mA/cm^2, Co-P-B-5 remains the best electrocatalyst. The HER and OER

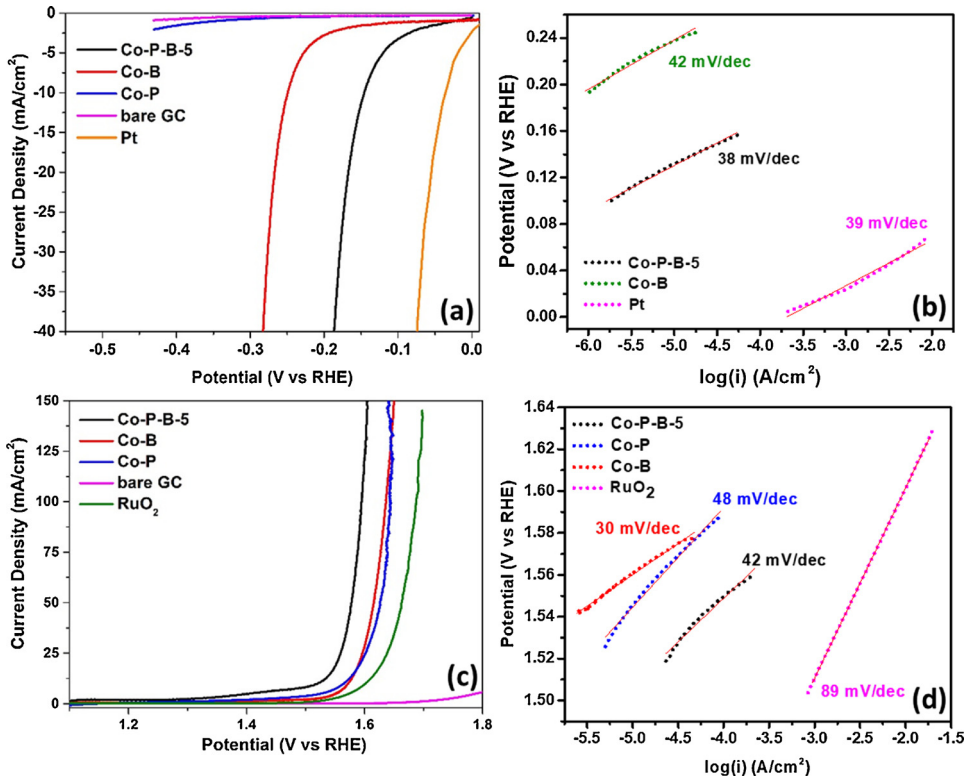

Fig. 3. Linear polarization curves (iR compensated) of Co-P-B-5, Co-B, Co-P and standard catalysts (Pt, RuO2) for **(a)** HER and **(c)** OER in pH 14, Tafel plots of Co-B, Co-P and Co-P-B-5 catalysts for **(b)** HER and **(d)** OER in pH 14.

performance obtained here for Co-P-B-5 catalyst is higher than those reported for other non-noble electrocatalysts such as Co-P-B/rGO [23], $Co_2B/CoSe_2$ [36], Co-Ni-B/NF [37], Co-P/CC [38], Fe-P nanorod array [39], etc. for HER and Co-P-B/rGO [23], Co-B/NCNT [40], Co-W-B/NF [41], Co-Fe-B/Cu sheet [42], etc. for OER. A more vivid comparison of the electrochemical performance of Co-P-B-5 with analogous non-noble catalysts from literature is presented in **Table S2**.

From above sections, it is firmly established that the amorphous Co-P-B-5 catalyst exhibits considerable improvement in the performance when used as cathode or anode in an alkaline water-splitting cell. To understand the intrinsic reasons for this improvement, it becomes necessary to investigate the material properties specifically related to the catalysis processes, and observe the changes induced due to the incorporation of P in Co-B. In catalysis, surface area plays a significant role as all the reactions take place on the surface of the catalyst. The physical surface area of the catalyst powders was determined using BET adsorption-desorption technique and the isotherms are shown in **Fig. S5**. All the curves belong to Type IV isotherm while resembling H3 type hysteresis loop, as per the IUPAC classification [43,44]. The surface area values of 22.8 m^2/g, 28.9 m^2/g and 62.9 m^2/g were obtained for Co-P-B-5, Co-B and Co-P, respectively. These values are consistent with the SEM images, where Co-P showed flake-like morphology, leading to higher surface area, while Co-B and Co-P-B-5 showed similar particle sizes. The lower surface area of Co-P-B-5, compared to Co-B, might be due to the higher degree of agglomeration, also evident in Fig. 1**c-d**. The inset graphs in Fig. S5 shows the pore-size distribution curves for all the three catalysts. The pore volume in Co-B and Co-P-B-5 catalysts is similar and very low when compared to Co-P, although the pore size distribution is pretty consistent in all cases. The higher pore volume in Co-P could also be one of the reasons for its higher surface area. In addition to the physical surface area, electroactive surface area (ESA) of the catalysts was also estimated, as it gives a true measure of the active sites present on the surface of the catalyst. ESA can be directly co-related to the double layer capacitance (C_{DL}) formed at the interface of the electrode and the electrolyte [30,45]. By carrying out CV scans at different scan rates in the non-Faradaic potential region, one can determine the values of C_{DL}. **Fig. S6** shows the CV scans for Co-B, Co-P-B-5 and Co-P at increasing scan rates of 20, 40, 60, 80 and 100 mV/s, measured in the potential window of -0.35 to -0.15 V in 1 M NaOH. From these CV curves, difference between the cathodic and anodic current densities were plotted against the scan rate (Fig. 4a) to obtain C_{DL} value. C_{DL} values of 0.065 m F/cm^2, 0.067 m F/cm^2 and 0.071 m F/cm^2 were obtained for Co-B, Co-P-B-5 and Co-P, respectively. It is interesting to note that the C_{DL} values and hence ESA of Co-B and Co-P-B-5 are very similar, indicating equal number of active sites on the surface. From BET values, it was seen that Co-P-B-5 has lower physical surface area than Co-B. However, Co-P-B-5 makes up for this shortcoming by presenting equal number of active sites on the surface, as Co-B. To explain this, the surface elemental composition obtained from XPS was considered (**Table S1**). The surface atomic content of Co is higher (~70%) in case of Co-P-B-5, as opposed to Co-B (~60%). Thus, addition of P in Co-B recreates the atomic arrangement to promote more number of Co atoms on the surface, also confirmed by ICP-AES results. This result is consistent with the other reports on Co-P-B powder synthesized by similar route [31,46]. These surface Co atoms are the active sites for adsorption of electrolytic species and hence explains the similar ESA for Co-B and Co-P-B-5. This also gives us a hint that the performance of Co-P-B-5 can be improved further, if the synthesis procedure can be tailored to hinder agglomeration of nanoparticles. This aspect will be investigated in our future work. One can also observe that Co-P has the highest concentration of Co on the surface (~92%) but it shows the lowest activity. This highlights the significance of B in enriching the Co active sites and also the fact that Co is not the active centre in Co-P.

From the discussion so far, it comes out that Co-P-B-5 has lower BET surface area but similar ESA to that of Co-B. On the other hand, Co-P has higher BET surface area and also higher ESA than that of Co-B and Co-P-B-5. However, the electrochemical performance for HER and OER,

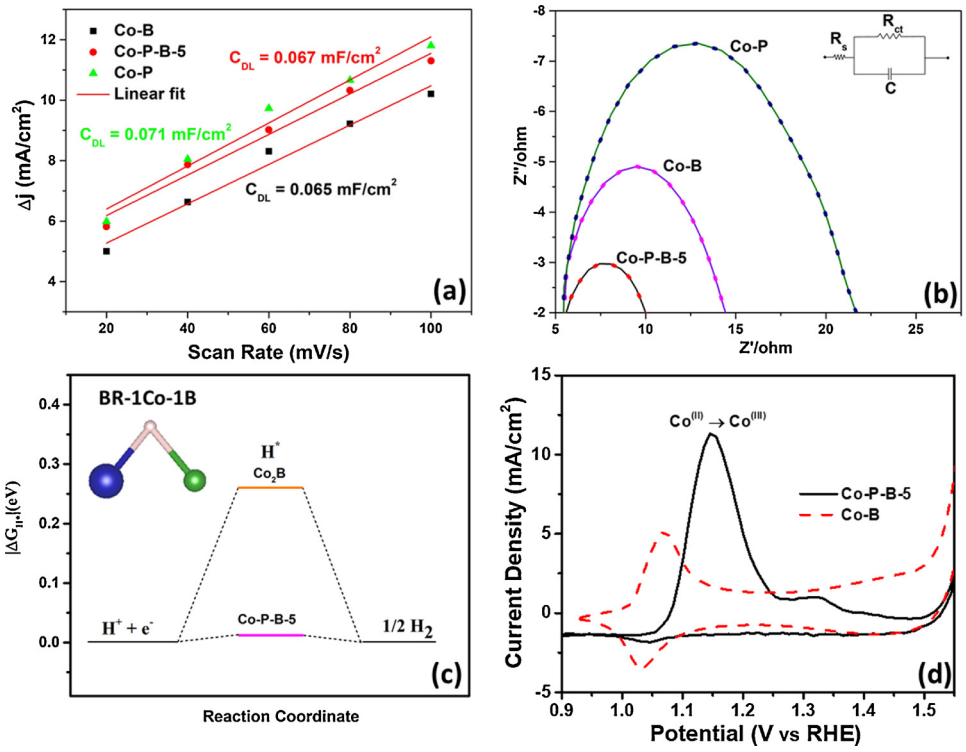

Fig. 4. (a) Plot representing the differences in cathodic and anodic current densities at -0.25 V versus scan rate to determine the double-layer capacitance (C_{DL}) of Co-B, Co-P and Co-P-B-5 catalysts; **(b)** Electrochemical impedance spectra (Nyquist curves) of Co-B, Co-P and Co-P-B-5 catalysts in 1 M NaOH, inset shows the equivalent circuit for the data; **(c)** Gibb's free energy diagram for bridge site (BR-1Co-1B) of Co_2B and Co-P-B-5 models, inset shows a schematic of BR-1Co-1B site (Blue sphere: cobalt, Green sphere: boron); **(d)** Cyclic voltammetry curves for Co-P-B-5 (solid line) and Co-B (dashed line) at a scan rate of 2 mV/s (For interpretation of the references to colour in this figure legend, the reader is referred to the web version of this article).

in pH 14, is the highest for Co-P-B-5, followed by Co-B and then by Co-P. A better understanding of the intrinsic activity of these catalysts can be obtained by removing the contribution from ESA. This was done by normalizing the obtained current with respect to C_{DL} values for each catalyst, as represented in **Fig. *S7***. It was observed that ESA normalized curves show exactly similar trend in HER and OER performances, as before, with Co-P-B-5 showcasing the highest intrinsic activity. This implies that the active sites in Co-P-B-5 are more active than that of Co-B and Co-P. To validate this speculation, turnover frequency (TOF) values were determined for all the three catalysts (**Table S3**), using a previously reported method [26,29]. For HER, TOF values of 0.0037, 0.0005 and 0.0141 atom^{-1}s^{-1} were obtained at 100 mV overpotential while for OER, TOF values 0.0863, 0.0231, and 0.1747 atom^{-1}s^{-1} were obtained at 500 mV overpotential, for Co-B, Co-P and Co-P-B-5, respectively. Thus, it becomes clear that the electrochemical performance at each active site on Co-P-B-5 is much higher than the same activity taking place on the active sites of Co-B and Co-P. Thus, incorporation of P in Co-B, not only promotes more number of Co atoms on the surface but also makes them more active for carrying out the water-splitting reactions.

Another crucial factor that can influence the electrochemical activity is the charge transfer resistance (R_{ct}) for a catalyst at the electrode/electrolyte interface. A quantitative value of R_{ct} was determined by fitting the Nyquist plots obtained from EIS with an appropriate equivalent circuit model. Fig. 4**b** shows the Nyquist plots for Co-B, Co-P and Co-P-B-5 recorded in pH 14 at an applied potential of 0.6 V. The corresponding equivalent circuit is illustrated in the inset of Fig. 4b, while the quantitative values obtained from fitting the graphs are tabulated in **Table S4**. One can observe that Co-P-B-5 exhibits the lowest R_{ct} value (5.88 Ω), followed by Co-B (9.04 Ω) and Co-P (16.18 Ω). It implies that charges are transferred across the electrode/electrolyte interface with least resistance in Co-P-B-5, owing to its higher conductivity. This would certainly lead to lower overpotential and hence higher reaction rates in Co-P-B-5, matching well with our results. Atomic and electronic rearrangement created by inclusion of P in Co-B also promotes better charge conductivity across the electrode and electrolyte interface.

To better understand the reasons for higher HER rate, DFT calculations were used. Amorphous Co_2B and Co-P-B-5 systems were simulated using VASP code [47–50] and their structural, electronic and magnetic properties were compared along with their H-adsorption capabilities. Owing to the fact that the amount of P is very small in Co-P-B-5 (B/P = 5), when P is added, it replaces the B sites rather than the transition metal sites and hence the density of states does not show any remarkable shift at the Fermi level. Addition of P also imparts a slightly higher magnetic moment (μ_B) to the Co-P-B-5 system (μ_B = 2.000) as against Co_2B (μ_B = 1.896). This explains the slightly higher degree of agglomeration and a lower value of BET surface area for Co-P-B-5 catalyst.

H-adsorption energies are established descriptors for predicting the catalytic ability of a material undergoing HER [3,21,51]. Hence, H-adsorption capability was studied at two different sites on Co_2B and Co-P-B-5 models, namely: top of individual atom and bridge sites (bond between 2 atoms). It was observed that the top site on P atom and the bridge sites involving P are not preferred for H adsorption. Similarly, the sites with excess B atoms are also observed to be undesirable for H-adsorption. In contrast, for Co_2P model, the most favourable sites are the ones involving P-atom, which agrees well with other reports on Co_2P [52], suggesting P to be the active centre for HER. In the case of Co-P-B-5, the gap between the bridge of one Co atom and one B atom (BR-1Co-1B) is the most preferred site for H-adsorption. Fig. 4**c** depicts the free energy diagram for Co_2B and Co-P-B-5 at the most favourable H-adsorption site (BR-1Co-1B). In the case of Co_2B, BR-1Co-1B depicts H-adsorption energy of -0.50 eV, which reduces drastically to -0.22 eV for Co-P-B-5, upon inclusion of P. This indicates that though P site is not preferred for H-adsorption, it helps in improving the H-adsorption capability of the Co containing sites. As results from XPS data, Co-P-B-5 inherits electron transfer mechanism analogous to Co-B and Co-P, wherein B loses electrons to Co while P gains electrons from Co. This unique interplay between Co, B and P modulates the electron density at Co sites and makes them optimum for H-adsorption. Thus, it can be inferred that higher electron density sites (as in Co-B) might not always be the most preferred site for H-adsorption as well. The modulated electronic density in Co-P-B-5 makes it suitable for H-adsorption and

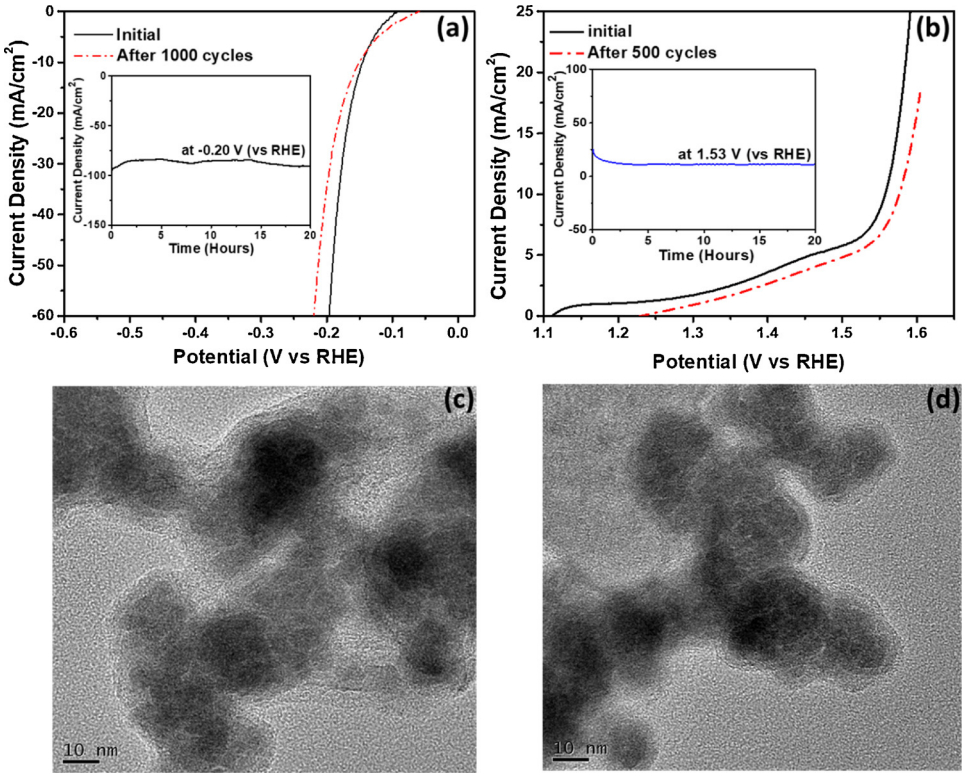

Fig. 5. Linear polarization curves of Co-P-B-5 before and after **(a)** 1000 cycles for HER and **(b)** 500 cycles for OER, in 1 M NaOH (pH 14) (at a scan rate of 100 mV/s), inset shows the chronoamperometric curves of Co-P-B-5 catalyst for HER and OER in pH 14, at fixed potentials; TEM images of Co-P-B-5 catalyst after long-term potentiostatic test for **(c)** HER and **(d)** OER, in 1 M KOH.

hence results in higher HER rate.

In case of metal borides and phosphides, it is very well established that the OER proceeds via formation of metal oxy/hydroxides on the surface of the catalyst [5,53]. The formation of surface species was investigated by carrying out CV scans in the pre-OER region for Co-B and Co-P-B-5 catalysts, at a scan rate of 2 mV/s (Fig. 4d). In both the catalysts, a primary oxidation peak is observed in the potential range of 1.05–1.15 V, which is reminiscent of the formation of CoOOH species [30,54,55] on the surface of the catalyst. The intensity of the oxidation peak is proportional to the amount of oxidized species generated on the surface. It can be seen that the degree of oxidation is much higher in case of Co-P-B-5, as compared to Co-B. As Co-P-B-5 has higher number of Co atoms on the surface, the formation of CoOOH species is higher and hence it facilitates OER to give lower overpotential.

The robustness of Co-P-B-5 towards HER and OER was established by carrying out durability tests and also testing it for HER under different pH solutions. Fig. 5**a** and **5b** shows the linear sweep curves of Co-P-B-5 before and after recycling tests for HER and OER respectively, in pH 14. For HER, the catalyst shows a slight increase in the overpotential (by 20 mV) after 1000 cycles. A similar increment was observed after 500 cycles of OER test, indicating negligible loss in performance. When used for industrial applications, the catalyst must sustain long hours of operation without replacement. Thus, Co-P-B-5 was maintained at a constant overpotential and a good stability in current density was observed for 20 h, both for HER (inset of Fig. 5a) and OER (inset of Fig. 5b) tests. **Fig. S8** shows the cathodic linear polarization curves for Co-P-B-5 in acidic and neutral solutions. Co-P-B-5 works in both these electrolytes and could achieve 10 mA/cm^2 at overpotentials of 295 mV and 178 mV in pH 1 and pH 7, respectively, thereby demonstrating its wide pH suitability. However, in acidic medium, visible deterioration of the catalyst was observed after a few tens of cycles due to leaching of the catalyst. In neutral medium, the catalyst remained extremely stable even after 20 h of potentiostatic test (**Fig. S9**) and 1000 cycles of operation (**Fig. S10**).

To understand the variation in morphology and chemical nature of Co-P-B-5 catalyst after subjecting to potentiostatic durability tests in alkaline medium, TEM and XPS characterizations were performed. TEM micrographs (**Fig. S11**) of the post-durability test samples denote excessive agglomeration of the particles, owing to the reaction conditions. Some sheet-like features were also seen in the images, which might be due to the contribution from polymeric binder used during the electrode preparation. High magnification TEM images in Fig. 5**c** and **5d** indicate that the spherical morphology of Co-P-B-5 nanoparticles remain intact after HER as well as OER tests. HR-TEM images (**Fig. S12**) show completely amorphous phases, confirming no structural transformation in the catalyst after HER and OER tests. The chemical states of each element in Co-P-B-5 after durability tests were investigated by obtaining XPS spectra (**Fig. S13**). Post HER durability test, BE peaks at 780.2, 781.8 eV and a satellite peak at 785.6 eV were observed for Co 2p states (**Fig. S13a**). This suggests that the surface oxides are transformed to higher oxidation states, which is expected due to the hydroxyl-rich alkaline environment. The important feature is the existence of metallic Co peak (777.9 eV), which is still preserved, as also seen in as-prepared samples. **Fig. S13b and S13c** represent the B 1 s and P 2p states of Co-P-B-5 catalyst after HER durability test, respectively. It was observed that boron is completely oxidised, and no signature of metallic boron was seen. The complete oxidation of boron and existence of metallic Co is perfectly in accordance with the fact that B donates electrons to Co and protects it against oxidation, keeping the Co sites active for HER. In case of P 2p states, two BE peaks at 129.4 and 133.3 eV were seen, which are attributed to metallic and oxidized phosphorous, respectively, similar to as-prepared samples. In case of post-OER test, Co 2p states exhibit BE peaks at 780.1 and 781.7 eV with a satellite peak at 786.0 eV (**Fig. S13d**). Here, no peak corresponding to metallic Co was observed, suggesting complete oxidation of the catalyst during OER. The obtained peaks correspond to Co^{3+} state alone, indicating dominance of CoOOH type species on the surface, which was also observed from CV scans (Fig.4d). This gives a direct evidence in support of our model that the formation of surface CoOOH species on Co-P-B-5 is the major factor facilitating OER. The BE peaks for B1 s state (**Fig. S13e**) is similar to that of as-prepared sample, suggesting no variation in chemical state of boron during OER. In case of P 2p state,

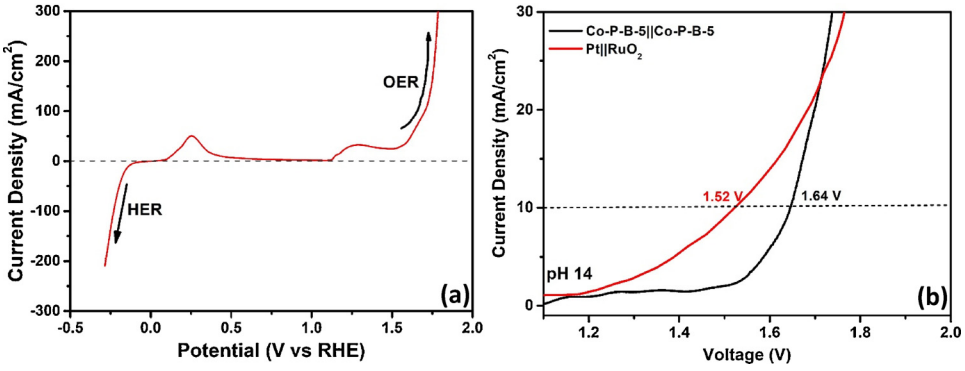

Fig. 6. (a) LSV curve for Co-P-B-5, scanned from cathodic end to anodic end, showing its ability to work as a bifunctional catalyst in pH 14; **(b)** Polarization curves for Co-P-B-5||Co-P-B-5 and RuO_2||Pt for overall water splitting in 1 M NaOH (2-electrode assembly).

only a single peak corresponding to oxidized phosphorous is seen (**Fig. S13f**).

The bifunctional nature of Co-P-B-5 was further demonstrated by running a linear sweep from cathodic region (-0.3 V) to anodic region (+1.7 V), as illustrated in Fig. 6**a**. To mimic industrial 2-electrode design, Co-P-B-5 was used as both cathode and anode in a 2-electrode system. In this 2-electrode assembly, a potential of 1.65 V was required to achieve the current density of 10 mA/cm^2 (Fig. 6b), which is slightly higher than that of Pt||RuO_2 assembly (1.52 V), under similar conditions. This demonstrates that Co-P-B-5 has excellent capabilities for overall water-splitting in alkaline medium, making it a unique candidate for up-scaling applications.

4. Conclusion

In summary, this work presents the development of a unique ternary catalyst in the form of Co-P-B, synthesized by a facile reduction method. After optimization, B/P molar ratio of 5 (Co-P-B-5) was found to be the most suitable proportion to have the best efficiency for HER and OER. Physical characterization revealed amorphous nature of Co-P-B-5 with similar morphology to that of Co-B. However, when tested for HER and OER, significant improvement in the performance was observed for Co-P-B-5 catalyst compared to Co-B and Co-P. XPS analysis indicated that Co-P-B-5 inherits electron transfer properties from Co-B as well as Co-P, wherein B loses electrons to Co while P gains electrons from Co. Electrochemical surface characterizations led to the conclusion that in spite of lower BET surface area, Co-P-B-5 presents equal number of surface active sites as Co-B, owing to the migration of Co atoms on the surface. Based on ESA normalized activity graphs and TOF values, it was seen that these surface Co atoms in Co-P-B-5 have higher intrinsic activity, when compared to Co-B and Co-P. DFT studies identified that the bridge site between a Co and B atom (BR-1Co-1B) is the most preferred site for H-adsorption in Co-P-B-5. Also, the H-adsorption energy at this bridge site is much lower (-0.22 eV) in the case of Co-P-B-5, as compared to Co_2B (-0.45 eV), confirming the role of P in modulating the electron density at Co sites for better H-adsorption and hence higher HER rate. CV scans, complemented by post-OER XPS data, confirmed that formation of CoOOH species on the surface of Co-P-B-5 is much higher, thereby facilitating OER. In the end, stability, recyclability and wide pH suitability of Co-P-B-5 was successfully demonstrated. This work presents a novel approach of combining two family of electrocatalysts, namely phosphides and borides to yield a new hybrid catalyst. Though this atomic compositional approach was tried by a few researchers, no concrete investigations were however carried out to isolate the roles of P and B in enhancing the reactions rates as, on the contrary, we did in this work. This work will pave way for more research activity to investigate new bridges between other families of electrocatalysts to achieve new benchmark overpotentials.

Declaration of Competing Interest

The authors declare that they have no known competing financial interests or personal relationships that could have appeared to influence the work reported in this paper.

Acknowledgements

A. Chunduri and N. Patel acknowledge WOS-A scheme (SR/WOS-A/PM-115/2016(C)) under DST for their financial support. N. Patel acknowledges UGC and SERB-DST for providing financial support through Faculty recharge program and Extra Mural project (**FILE NO.** EMR/2016/003028). S. Gupta acknowledges the research grant from UK Commonwealth Commission through Commonwealth Rutherford Fellowship (INRF-2017-139). M. K. Patel acknowledges the seed funding obtained from EPSRC-GCRF No. 141131/155337.

Appendix A. Supplementary data

Supplementary material related to this article can be found, in the online version, at doi:https://doi.org/10.1016/j.apcatb.2019.118051.

References

[1] M. Zeng, Y. Li, Recent advances in heterogeneous electrocatalysts for the hydrogen evolution reaction, J. Mater. Chem. A Mater. Energy Sustain. 3 (2015) 14942–14962.
[2] O. Khaselev, J.A. Turner, A monolithic photovoltaic-photoelectrochemical device for hydrogen production via water splitting, Science 280 (80) (1998) 425–427.
[3] Y. Jiao, Y. Zheng, M. Jaroniec, S.Z. Qiao, Design of electrocatalysts for oxygen-and hydrogen-involving energy conversion reactions, Chem. Soc. Rev. 44 (2015) 2060–2086.
[4] N.-T. Suen, S.-F. Hung, Q. Quan, N. Zhang, Y.-J. Xu, H.M. Chen, Electrocatalysis for the oxygen evolution reaction: recent development and future perspectives, Chem. Soc. Rev. 46 (2017) 337–365.
[5] J.S. Kim, B. Kim, H. Kim, K. Kang, Recent progress on multimetal oxide catalysts for the oxygen evolution reaction, Adv. Energy Mater. 8 (2018) 1702774, , https://doi.org/10.1002/aenm.201702774.
[6] Y. Lee, J. Suntivich, K.J. May, E.E. Perry, Y. Shao-Horn, Synthesis and activities of rutile IrO2 and RuO2 nanoparticles for oxygen evolution in acid and alkaline solutions, J. Phys. Chem. Lett. 3 (2012) 399–404.
[7] E.J. Popczun, J.R. McKone, C.G. Read, A.J. Biacchi, A.M. Wiltrout, N.S. Lewis, R.E. Schaak, Nanostructured nickel phosphide as an electrocatalyst for the hydrogen evolution reaction, J. Am. Chem. Soc. 135 (2013) 9267–9270.
[8] P. Jiang, Q. Liu, C. Ge, W. Cui, Z. Pu, A.M. Asiri, X. Sun, CoP nanostructures with different morphologies: synthesis, characterization and a study of their electrocatalytic performance toward the hydrogen evolution reaction, J. Mater. Chem. A Mater. Energy Sustain. 2 (2014) 14634–14640.
[9] S. Gupta, N. Patel, A. Miotello, D.C. Kothari, Cobalt-Boride: an efficient and robust electrocatalyst for hydrogen evolution reaction, J. Power Sources 279 (2015) 620–625, https://doi.org/10.1016/j.jpowsour.2015.01.009.
[10] J. Masa, I. Sinev, H. Mistry, E. Ventosa, M. de la Mata, J. Arbiol, M. Muhler, B. Roldan Cuenya, W. Schuhmann, Ultrathin high surface area nickel boride (NixB) nanosheets as highly efficient electrocatalyst for oxygen evolution, Adv. Energy Mater. 7 (2017) 1700381.
[11] X. Geng, W. Sun, W. Wu, B. Chen, A. Al-Hilo, M. Benamara, H. Zhu, F. Watanabe, J. Cui, T. Chen, Pure and stable metallic phase molybdenum disulfide nanosheets for hydrogen evolution reaction, Nat. Commun. 7 (2016) 10672.
[12] Y. Li, Y. Yu, Y. Huang, R.A. Nielsen, W.A. Goddard III, Y. Li, L. Cao, Engineering the

composition and crystallinity of molybdenum sulfide for high-performance electrocatalytic hydrogen evolution, ACS Catal. 5 (2014) 448–455.
[13] B. Qu, X. Yu, Y. Chen, C. Zhu, C. Li, Z. Yin, X. Zhang, Ultrathin MoSe2 nanosheets decorated on carbon fiber cloth as binder-free and high-performance electrocatalyst for hydrogen evolution, ACS Appl. Mater. Interfaces 7 (2015) 14170–14175.
[14] M.-R. Gao, Z.-Y. Lin, T.-T. Zhuang, J. Jiang, Y.-F. Xu, Y.-R. Zheng, S.-H. Yu, Mixed-solution synthesis of sea urchin-like NiSe nanofiber assemblies as economical Pt-free catalysts for electrochemical H 2 production, J. Mater. Chem. 22 (2012) 13662–13668.
[15] F. Harnisch, G. Sievers, U. Schröder, Tungsten carbide as electrocatalyst for the hydrogen evolution reaction in pH neutral electrolyte solutions, Appl. Catal. B Environ. 89 (2009) 455–458.
[16] Y. Liu, G. Yu, G. Li, Y. Sun, T. Asefa, W. Chen, X. Zou, Coupling Mo2C with nitrogen-rich nanocarbon leads to efficient hydrogen-evolution electrocatalytic sites, Angew. Chemie Int. Ed. 54 (2015) 10752–10757.
[17] B. You, N. Jiang, M. Sheng, S. Gul, J. Yano, Y. Sun, High-performance overall water splitting electrocatalysts derived from cobalt-based metal–organic frameworks, Chem. Mater. 27 (2015) 7636–7642.
[18] Q. Liu, S. Gu, C.M. Li, Electrodeposition of nickel–phosphorus nanoparticles film as a Janus electrocatalyst for electro-splitting of water, J. Power Sources 299 (2015) 342–346.
[19] P. Xiao, M.A. Sk, L. Thia, X. Ge, R.J. Lim, J.-Y. Wang, K.H. Lim, X. Wang, Molybdenum phosphide as an efficient electrocatalyst for the hydrogen evolution reaction, Energy Environ. Sci. 7 (2014) 2624–2629, https://doi.org/10.1039/C4EE00957F.
[20] H. Li, P. Wen, Q. Li, C. Dun, J. Xing, C. Lu, S. Adhikari, L. Jiang, D.L. Carroll, S.M. Geyer, Earth-abundant Iron diboride (FeB2) nanoparticles as highly active bifunctional electrocatalysts for overall water splitting, Adv. Energy Mater. 7 (2017) 1700513, , https://doi.org/10.1002/aenm.201700513.
[21] P. Liu, J.A. Rodriguez, Catalysts for hydrogen evolution from the [NiFe] hydrogenase to the Ni2P (001) surface: the importance of ensemble effect, J. Am. Chem. Soc. 127 (2005) 14871–14878.
[22] P. Zhang, M. Wang, Y. Yang, T. Yao, H. Han, L. Sun, Electroless plated Ni–Bx films as highly active electrocatalysts for hydrogen production from water over a wide pH range, Nano Energy 19 (2016) 98–107, https://doi.org/10.1016/j.nanoen.2015.11.020.
[23] P. Li, Z. Jin, D. Xiao, A one-step synthesis of Co–P–B/rGO at room temperature with synergistically enhanced electrocatalytic activity in neutral solution, J. Mater. Chem. A Mater. Energy Sustain. 2 (2014) 18420–18427.
[24] J. Kim, H. Kim, S.-K. Kim, S.H. Ahn, Electrodeposited amorphous Co–P–B ternary catalyst for hydrogen evolution reaction, J. Mater. Chem. A Mater. Energy Sustain. 6 (2018) 6282–6288.
[25] H. Sun, X. Xu, Z. Yan, X. Chen, L. Jiao, F. Cheng, J. Chen, Superhydrophilic amorphous Co–B–P nanosheet electrocatalysts with Pt-like activity and durability for the hydrogen evolution reaction, J. Mater. Chem. A Mater. Energy Sustain. 6 (2018) 22062–22069.
[26] S. Gupta, N. Patel, R. Fernandes, R. Kadrekar, A. Dashora, A.K. Yadav, D. Bhattacharyya, S.N. Jha, A. Miotello, D.C. Kothari, Co–Ni–B nanocatalyst for efficient hydrogen evolution reaction in wide pH range, Appl. Catal. B Environ. 192 (2016) 126–133.
[27] H. Park, Y. Zhang, J.P. Scheifers, P.R. Jothi, A. Encinas, B.P.T. Fokwa, Graphene- and phosphorene-like boron layers with contrasting activities in highly active Mo2B4 for hydrogen evolution, J. Am. Chem. Soc. 139 (2017) 12915–12918.
[28] M. Ma, F. Qu, X. Ji, D. Liu, S. Hao, G. Du, A.M. Asiri, Y. Yao, L. Chen, X. Sun, Bimetallic nickel-substituted cobalt-borate nanowire array: an earth-abundant water oxidation electrocatalyst with superior activity and durability at near neutral pH, Small. 13 (2017) 1700394.
[29] S. Gupta, N. Patel, R. Fernandes, S. Hanchate, A. Miotello, D.C. Kothari, Co-Mo-B nanoparticles as a non-precious and efficient bifunctional electrocatalyst for hydrogen and oxygen evolution, Electrochim. Acta 232 (2017) 64–71.
[30] S. Gupta, A. Yadav, S. Bhartiya, M.K. Singh, A. Miotello, A. Sarkar, N. Patel, Co oxide nanostructures for electrocatalytic water-oxidation: effects of dimensionality and related properties, Nanoscale. 10 (2018) 8806–8819.
[31] N. Patel, R. Fernandes, A. Miotello, Hydrogen generation by hydrolysis of NaBH4 with efficient Co–P–B catalyst: a kinetic study, J. Power Sources 188 (2009) 411–420.
[32] J. Yang, H. Liu, W.N. Martens, R.L. Frost, Synthesis and characterization of cobalt hydroxide, cobalt oxyhydroxide, and cobalt oxide nanodiscs, J. Phys. Chem. C. 114 (2009) 111–119.
[33] Y. Pan, Y. Lin, Y. Chen, Y. Liu, C. Liu, Cobalt phosphide-based electrocatalysts: synthesis and phase catalytic activity comparison for hydrogen evolution, J. Mater. Chem. A Mater. Energy Sustain. 4 (2016) 4745–4754.
[34] H.-W. Liang, S. Brüller, R. Dong, J. Zhang, X. Feng, K. Müllen, Molecular metal–Nx centres in porous carbon for electrocatalytic hydrogen evolution, Nat. Commun. 6 (2015) 7992, https://doi.org/10.1038/ncomms8992.
[35] E.J. Popczun, C.G. Read, C.W. Roske, N.S. Lewis, R.E. Schaak, Highly active electrocatalysis of the hydrogen evolution reaction by cobalt phosphide nanoparticles, Angew. Chemie Int. Ed. 53 (2014) 5427–5430, https://doi.org/10.1103/PhysRevB.47.558.
[36] Y. Guo, Z. Yao, C. Shang, E. Wang, Amorphous Co2B grown on CoSe2 nanosheets as a hybrid catalyst for efficient overall water splitting in alkaline medium, ACS Appl, Mater. Interfaces. 9 (2017) 39312–39317.
[37] N. Xu, G. Cao, Z. Chen, Q. Kang, H. Dai, P. Wang, Cobalt nickel boride as an active electrocatalyst for water splitting, J. Mater. Chem. A Mater. Energy Sustain. 5 (2017) 12379–12384.
[38] J. Tian, Q. Liu, A.M. Asiri, X. Sun, Self-supported nanoporous cobalt phosphide nanowire arrays: an efficient 3D hydrogen-evolving cathode over the wide range of pH 0–14, J. Am. Chem. Soc. 136 (2014) 7587–7590.
[39] Y. Liang, Q. Liu, A.M. Asiri, X. Sun, Y. Luo, Self-supported FeP nanorod arrays: a cost-effective 3D hydrogen evolution cathode with high catalytic activity, ACS Catal. 4 (2014) 4065–4069.
[40] K. Elumeeva, J. Masa, D. Medina, E. Ventosa, S. Seisel, Y.U. Kayran, A. Genç, T. Bobrowski, P. Weide, J. Arbiol, Cobalt boride modified with N-doped carbon nanotubes as a high-performance bifunctional oxygen electrocatalyst, J. Mater. Chem. A Mater. Energy Sustain. 5 (2017) 21122–21129.
[41] G. Cao, N. Xu, Z. Chen, Q. Kang, H. Dai, P. Wang, Cobalt-tungsten-Boron as an active electrocatalyst for water electrolysis, Chem. Select. 2 (2017) 6187–6193.
[42] H. Chen, S. Ouyang, M. Zhao, Y. Li, J. Ye, Synergistic activity of Co and Fe in amorphous Co x–Fe–B catalyst for efficient oxygen evolution reaction, ACS Appl. Mater. Interfaces 9 (2017) 40333–40343.
[43] I. Recommendations, Pure appl. IUPAC recommendations, Pure Appl. Chem. 57 (1985) 603.
[44] K.S.W. Sing, IUPAC Recommendations 1994 for Reporting Physisorption Data, Pure Appl. Chem. 66 (1994) 1739.
[45] S.K. Singh, V.M. Dhavale, S. Kurungot, Low surface energy plane exposed Co3O4 nanocubes supported on nitrogen-doped graphene as an electrocatalyst for efficient water oxidation, ACS Appl. Mater. Interfaces 7 (2014) 442–451.
[46] H. Li, P. Yang, D. Chu, H. Li, Selective maltose hydrogenation to maltitol on a ternary Co–P–B amorphous catalyst and the synergistic effects of alloying B and P, Appl. Catal. A Gen. 325 (2007) 34–40.
[47] G. Kresse, J. Hafner, Ab initio molecular dynamics for liquid metals, Phys. Rev. B 47 (1993) 558–561, https://doi.org/10.1103/PhysRevB.47.558.
[48] G. Kresse, J. Hafner, Ab initio molecular-dynamics simulation of the liquid-metal–amorphous-semiconductor transition in germanium, Phys. Rev. B 49 (1994) 14251–14269, https://doi.org/10.1103/PhysRevB.49.14251.
[49] G. Kresse, J. Furthmüller, Efficient iterative schemes for ab initio total-energy calculations using a plane-wave basis set, Phys. Rev. B 54 (1996) 11169–11186, https://doi.org/10.1103/PhysRevB.54.11169.
[50] G. Kresse, J. Furthmüller, Efficiency of ab-initio total energy calculations for metals and semiconductors using a plane-wave basis set, Comput. Mater. Sci. 6 (1996) 15–50, https://doi.org/10.1016/0927-0256(96)00008-0.
[51] Y. Zheng, Y. Jiao, Y. Zhu, L.H. Li, Y. Han, Y. Chen, A. Du, M. Jaroniec, S.Z. Qiao, Hydrogen evolution by a metal-free electrocatalyst, Nat. Commun. 5 (2014) 3783.
[52] G. Hu, Q. Tang, D. Jiang, CoP for hydrogen evolution: implications from hydrogen adsorption, Phys. Chem. Chem. Phys. 18 (2016) 23864–23871.
[53] E. Fabbri, A. Habereder, K. Waltar, R. Kötz, T.J. Schmidt, Developments and perspectives of oxide-based catalysts for the oxygen evolution reaction, Catal. Sci. Technol. 4 (2014) 3800–3821.
[54] W.K. Behl, J.E. Toni, Anodic oxidation of cobalt in potassium hydroxide electrolytes, J. Electroanal. Chem. Interfacial Electrochem. 31 (1971) 63–75.
[55] E. Potvin, L. Brossard, Oxygen evolution on electrochemically generated cobalt spinel coating, J. Appl. Electrochem. 25 (1995) 462–471.